Wu, L., Hou, C., Wang, X., **Guo, P.**, Zhang, X., Jin, Y., Gong, Y., Chen, X., Li, H. (2023): New insights into the mechanism for $^1O_2$-Dominated peroxymonosulfate activation in saline solution: In-situ generation of H_2O_2 to inhibit the AOX formation
Chem. Eng. J. **474** , art. 145698

New Insights into the Mechanism for $^1O_2$-Dominated Peroxymonosulfate Activation in Saline Solution：In-situ Generation of H_2O_2 to Inhibit the AOX Formation

Liyuan Wu[a]*, Chenjing Hou[a], Xin Wang[a], Pengpeng Guo[b], Xiaoran Zhang[a], Yi Jin[c] , Yongwei Gong[a] , Xudan Chen[a] and Haiyan Li[a]

[a] Beijing Engineering Research Center of Sustainable Urban Sewage System Construction and Risk Control, Beijing University of Civil Engineering and Architecture, Beijing, 100044, China

[b] Helmholtz Centre for Environmental Research-UFZ, Department of Environmental Engineering, Leipzig, 04318

[c] Power China Beijing Engineering Corporation Limited, Beijing, 100024, China

Email: wuliyuan@bucea.edu.cn (Liyuan Wu)

Abstract: The presence of chloride ions (Cl^-) in dye wastewater can hinder the peroxymonosulfate (PMS) oxidation and lead to the abundant production of toxic adsorbable organic halogens (AOX). In this study, we investigate the detailed influence of Cl^- on RhB removal and its mechanism, and propose a potential pathway for $^1O_2$-dominated systems to inhibit AOX formation. The concentration of Cl^- has a dual effect on the degradation of RhB, with low

concentrations inhibiting and high concentrations promoting. Further studies have revealed that Cl^- significantly impact the generation and transformation of reactive oxygen species (ROSs). EPR capturing, quenching tests, and molecular probe experiments indicate that as the Cl^- concentration increases, the concentration of $SO_4^{\bullet-}$, $^{\bullet}OH$ and their contribution to the degradation of RhB gradually decrease, $^1O_2$ slightly increase and then decrease, while HClO and chlorine radicals increase linearly. Additionally, the catalyst plays a crucial role in inhibiting AOX formation and improving the mineralization of RhB. On the one hand, introducing catalysts can alter the proportion of ROSs production. On the other hand, the in-situ generation of H_2O_2 on the catalyst surface, through O_2 adsorption at sulfur vacancies sites, consumes the produced HClO, thereby inhibiting the formation of AOX. This study proposed a new insight into the mechanism for effective reduction of AOX content for $^1O_2$ dominated non-radical PMS activation under saline water.

Keywords: peroxymonosulfate, chloride ions, hypochlorite, adsorbable organic halogen, hypochlorous acid

Graphic abstract

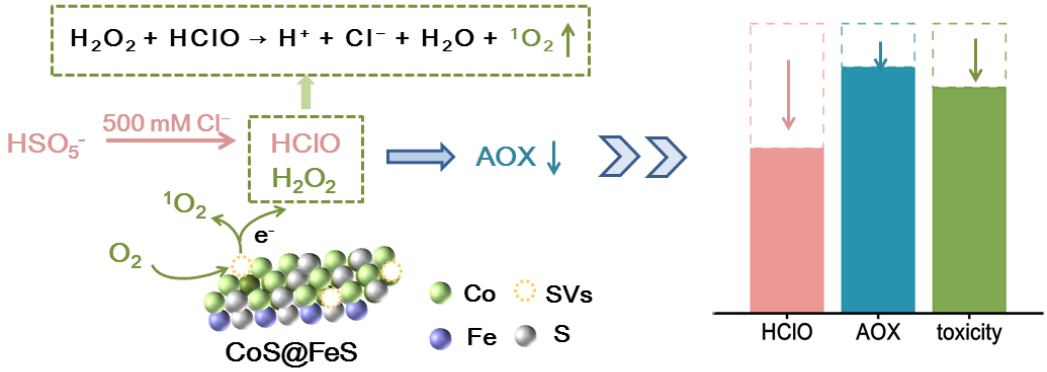

1 Introduction

Recently, the advanced oxidation processes (AOPs) through peroxymonosulfate (PMS) activation have gained great attention [1], due to its ability to produce various reactive oxidative species [2-6]. However, the practical application of PMS activation is usually limited by the presence of co-existing anions (such as Cl^-) in real wastewater matrix. The coexisting Cl^- can quench the $SO_4^{\bullet-}$ and $^{\bullet}OH$, resulting in the formation of less oxidative chlorine radicals (RCSs, such as $Cl^{\bullet}$, $ClO^{\bullet}$, and $Cl_2^{\bullet-}$) (Eqs. 1–4) [7]. These RCSs can readily bond with the unsaturated bonds of the contaminants and produce adsorbable organic halogens (AOX) [8, 9], which are highly toxic and difficult for further degradation [10, 11]. Additionally, Cl^- could also react with HSO_5^- (Eqs. 5–6), leading to the production of HClO or Cl_2 through a two-step electron transfer pathway [12]. The subsequent direct chlorination of aromatic rings of the organic pollutants can also generate a large amount of AOX [8, 13, 14].

In order to prevent the formation of AOX during PMS activation in Cl^- containing system, utilizing the non-radical pathway through singlet oxygen ($^1O_2$) is considered as a possible solution [15-19], due to the sluggishness of $^1O_2$ towards Cl^- ($k_{^1O_2,\ Cl^-}$ = 1×10^3 $M^{-1}s^{-1}$). The amount of AOX in $^1O_2$-dominated PMS activation systems is typically low in saline solution [10]. However, under high Cl^- concentration, the generation of $^1O_2$ is greatly suppressed [20, 21]. Since Cl^- can easily react with HSO_5^- and formed into HClO, then decrease the amount of $^1O_2$ produced by PMS self-decomposition, finally taken instead of the dominant contribution role of $^1O_2$ [22]. Thus, the explanation for the reduction of AOX in $^1O_2$-dominated systems that attributed to the low reactivity of $^1O_2$ and Cl^- seems to be untenable [10]. To clearly address the issue of AOX formation in saline wastewater, it is imperative to conduct thorough research to understand the regularity of the transformation of the reactive species, and seek the underlying mechanism for AOX inhibition in the $^1O_2$-dominated PMS catalysis.

$$Cl^- + {}^{\bullet}OH \rightarrow ClOH^{\bullet-} \qquad k = 0.43–5.81\times10^{10}\ M^{-1}s^{-1} \qquad (1)$$

$$ClOH^{\bullet-} + H^+ \rightarrow Cl^{\bullet} + H_2O \qquad k = 2.1\times10^{10}\ M^{-1}s^{-1} \qquad (2)$$

$$Cl^- + SO_4^{\bullet-} \rightarrow SO_4^{2-} + Cl^{\bullet} \qquad k = 0.27 – 6.35\times10^{9}\ M^{-1}s^{-1} \qquad (3)$$

$$Cl^{\bullet} + Cl^- \rightarrow Cl_2^{\bullet-} \qquad k = 0.65–8.78\times10^{10}\ M^{-1}s^{-1} \qquad (4)$$

$$Cl^- + HSO_5^- \rightarrow SO_4^{2-} + HClO \qquad k = 2.1\times10^{-3}\ M^{-1}s^{-1} \qquad (5)$$

$$HClO \rightleftharpoons H^+ + ClO^- \qquad pK_a = 7.5 \qquad (6)$$

In our previous study, we fabricated the CoS@FeS heterostructure catalyst with sulfur vacancies (SVs) using a simple hydrothermal strategy. Various characterization methods were employed to analyze the materials, including X-ray photoelectron spectroscopy (XPS), EPR spectra of sulfur vacancies, scanning electron microscopy (SEM), high-resolution transmission electron microscopy (HRTEM), etc.[21]. Mechanism studies have revealed that the SVs facilitate the adsorption of O_2, then O_2 acquire electrons to generate $O_2^{\bullet-}$, which is favorable for the production of $^1O_2$. On this basis, we further investigated the impact of Cl^- concentration (0–500 mM） on the RhB removal. The transformation of reactive species, particularly $^1O_2$ and RCSs, in the CoS@FeS/PMS system was elucidated, according to the comparative studies of the EPR capturing, quenching experiments, and probe conversion experiments under different Cl^- concentrations. Then, the variations of H_2O_2, HClO and AOX concentration under different dose of catalyst and Cl^- concentration were measured to reveal the role of catalyst. Based on the above research, the important role of in-situ generation of H_2O_2 on the catalyst for consuming the HClO in PMS activation under saline condition was first time proposed and verified. This study clarified the Cl^- influence under different concentrations as well as the possible mechanism, and put forward the importance of in-situ generated H_2O_2 for AOX inhibition for $^1O_2$ -dominated PMS activation.

2 Materials and methods

2.1 Chemicals and Reagents

Methanol (MeOH), sodium chloride (NaCl) and hydrogen peroxide (H_2O_2, ≥30.0%) were obtained from Sinopharm Chemical Reagent Co., Ltd. Peroxymonosulfate (PMS) was purchased from Alfa Aesar Chemical Co., Ltd. Rhodamine B (RhB) as target pollutant was acquired from Aladdin Biochemical Technology Co., Ltd. Details of other reagents was listed in S1. All chemicals were analytically pure and used without further purification. All catalysis reactions were carried out with deionized water.

2.2 Preparation of Catalysts

CoS@FeS nanosheets heterostructure catalyst was synthesized by a simple hydrothermal method. L-Cysteine, $Co(SO_4)_2 \cdot 6H_2O$ and $(NH_4)_2Fe(SO_4)_2 \cdot 6H_2O$ were dissolved in mixture solution (25 mL deionized and 25 ml triethylenetetramine) and heated at 200 ℃ for 24 hours. The detailed synthesis of the CoS@FeS was described according to our previous work (S2) [21]. The characterization information of the material is in S3–4.

2.3 Experiment procedure

2.3.1 The degradation of RhB in CoS@FeS/PMS/ Cl^- system

A series of 100 mL RhB (20 mg/L) solutions containing NaCl of 0, 5, 10, 20, 50, 100, 300, and 500 mM were prepared in a 250 mL beaker, respectively. For each entry, 2 mg of the catalyst CoS@FeS was added to the RhB solution and stirred for 10 min. Then, 1 mL of PMS reagents (100 mM) was added to initiate the RhB degradation. Meanwhile, 0.5 mL of the above solution was extracted from the beaker at the fixed time intervals and immediately quenched with 0.5 mL Na_2SO_3 (100 mM), filtered with a 0.22 μm membrane, then detected by a UV-Vis spectrophotometer to analyze the concentration of RhB. All experiments were performed at 25 ℃. For pH effect studies, the initial solution pH was adjusted by NaOH (0.01 M) and H_2SO_4 (0.01 M) if necessary.

2.3.2 Determination of rate constant for the reaction of RhB

The second-order rate constants for the reaction of RhB with $SO_4^{\bullet-}$, $^{\bullet}OH$, and $^1O_2$ were measured by the competition kinetics method. The detailed experimental procedure and calculation method were described in Text S5–S7.

2.3.3 Determination of the steady-state concentration of ROSs

To determine the steady-state concentration of ROSs ($SO_4^{\bullet-}$, $^{\bullet}OH$, and $^1O_2$), CoS@FeS, PMS, and RhB were introduced into various NaCl containing solutions. Sulfamethoxazole (SMX), nitrobenzene (NB), and Metronidazole (MDE) as kinetic probe were added in the CoS@FeS/PMS system [23-25]. To mitigate the impact of RCSs and HClO on the degradation of organic matter in a high concentration Cl^-

system, the reaction solution was supplemented with $NaHCO_3$ and $(NH_4)_2SO_4$. The steady-state concentration of ROSs in the system was assessed by Eqs 7–9. The second order rate constants of SMX, NB, and MDE with ROSs are detailed in S8.

$$-\ln\frac{[SMX]}{[SMX]_0} = k_{SMX,\ SO_4^{\bullet-}}[SO_4^{\bullet-}]_{ss} + k_{SMX,\ {}^{\bullet}OH}[{}^{\bullet}OH]_{ss} + k_{SMX,\ {}^1O_2}[{}^1O_2]_{ss} \quad (7)$$

$$-\ln\frac{[NB]}{[NB]_0} = k_{NB,\ SO_4^{\bullet-}}[SO_4^{\bullet-}]_{ss} + k_{NB,\ {}^{\bullet}OH}[{}^{\bullet}OH]_{ss} + k_{NB,\ {}^1O_2}[{}^1O_2]_{ss} \quad (8)$$

$$-\ln\frac{[MDE]}{[MDE]_0} = k_{MDE,\ SO_4^{\bullet-}}[SO_4^{\bullet-}]_{ss} + k_{MDE,\ {}^{\bullet}OH}[{}^{\bullet}OH]_{ss} + k_{MDE,\ {}^1O_2}[{}^1O_2]_{ss} \quad (9)$$

Where $k_{SMX,\ SO_4^{\bullet-}}$, $k_{SMX,,{}^{\bullet}OH}$ and $k_{SMX,{}^1O_2}$ are the second order rate constants for the reaction of SMX with $SO_4^{\bullet-}$,$^{\bullet}OH$ and $^1O_2$; $k_{NB,SO_4^{\bullet-}}$, $k_{NB,{}^{\bullet}OH}$, and $k_{NB,{}^1O_2}$ are the second order rate constants for the reaction of NB with $SO_4^{\bullet-}$,$^{\bullet}OH$ and $^1O_2$; $k_{MDE,SO_4^{\bullet-}}$, $k_{MDE,{}^{\bullet}OH}$ and $k_{MDE,{}^1O_2}$ are the second order rate constants for the reaction of MDE with $SO_4^{\bullet-}$,$^{\bullet}OH$ and $^1O_2$. $[SO_4^{\bullet-}]_{ss}$, $[{}^{\bullet}OH]_{ss}$, $[{}^1O_2]_{ss}$ are the steady-state concentration of $SO_4^{\bullet-}$,$^{\bullet}OH$ and $^1O_2$, respectively.

2.4 Analytical Methods

The concentration of RhB for each sample was detected by a UV-Vis spectrophotometer (PerkinElmer, Lambda 950) with a detection wavelength of 554 nm. The total organic carbon (TOC) was measured by TOC–Analyzer (multi–N/C3100, Analytik Jena, Germany). EPR experiments were performed on a JEOL JES–FA200 spectrometer, sulfate radical ($SO_4^{\bullet-}$), hydroxyl radical ($^{\bullet}OH$), and superoxide radical ($O_2^{\bullet-}$) were identified using DMPO as spin trapping agent. Singlet

oxygen ($^1O_2$) and chlorine Radicals ($Cl_2^{\bullet-}$) were detected using TEMP andα-phenyl-N-tert-butylnitronone (PBN) as the spin-trapping agent. The quenching experiment was similar to the target pollutants degradation experiment, except for the addition of the corresponding quenchers (methanol, tert-butanol, isopropanol, ammonium sulfate, β-carotene) before adding PMS. The detection of the concentrations of free chlorine ($HClO/ClO^-$) was measured by *N*,*N*-diethyl-p-phenylenediamine (DPD) method. A benchtop UV spectrophotometer (DR3900, HACH) measures the absorbance of magenta-colored compounds at a wavelength of 515 nm. The concentration of the adsorbable organic halogen (AOX) was analyzed by a combustion furnace (AOX-C, Blue Sky Instruments, China) and ion chromatograph (CIC-D100, Qingdao Shenghan, China), and the determined sample was adsorbed by activated carbon for advance. The analysis for the RhB intermediates after degradation was performed on the Agilent LC1290-6550-QTOF instrument. The mobile phase was 0.1% formic acid and 100% methanol, and the column model was Agilent RRHD Eclipse Plus C18 (2.1 mm × 100 mm × 1.8 μm).

The concentration of H_2O_2 used N, N-diethyl-p-phenylenediamine sulfate (DPD)/peroxidase (POD) method. Firstly, 50 mg of DPD was dissolved in 5 mL of 0.1 mol/L H_2SO_4 water to create the DPD solution. Next, 5 mg of POD was dissolved in 5 mL of deionized water to create the POD solution. Then, mixed 1 mL of the sample solution with 0.05 mL of DPD solution, 0.05 mL of POD solution, and 1 mL

of sodium phosphate buffer (0.1 mol/L, pH = 6.0). Finally, determined the concentration of H_2O_2 by measuring the absorbance at λ = 551 nm using a UV-Vis spectrophotometer (PerkinElmer, Lambda 950). The concentration of SMX, NB, and MDE were determined using high performance liquid chromatography (HPLC, Agilent). The specific test conditions can be found in S9.

3 Results and discussion

3.1 The degradation of RhB

3.1.1 In the absence of Cl^-

Initially, the reaction parameters of CoS@FeS/PMS activation for RhB degradation, including different PMS concentrations, catalyst dosages, and initial pH were optimized in the absence of Cl^-. Results showed that the best RhB removal could be reached 98.64 % within 30 minutes under pH 6.4, 20 mg/L of RhB, 1 mM of PMS and 20 mg/L of catalyst, with the observed pseudo-first-order rate constant (k_{obs}) of 0.143 min^{-1}. Additionally, the catalysis could maintain a high level of RhB removal even after five catalysis cycles (95%), demonstrating its good reusability, as detailed in the Text S10–S13. All the subsequent entries were operated under the above optimized condition.

3.1.2 Under different [Cl^-]

The presence of co-existing ions poses a challenge for the practical application of PMS oxidation [26, 27]. To investigate the impact of Cl^- concentrations on RhB removal, an elaborate concentration range of Cl^- solutions of 0, 5, 10, 20, 50, 100, 300, and 500 mM were set. It was observed that Cl^- has a dual effect on RhB degradation (S114), decreased slightly under low [Cl^-] (0–10 mM) and began to increase during high [Cl^-] of 20–500 mM. The k_{obs} decreased from 0.143 to 0.119 min^{-1} during 0–10 mM [Cl^-], and increased to 0.767 min^{-1} during 20–500 mM [Cl^-] (Fig. 1a), similar tendencies were also reported in literatures [28-30]. Previous studies have indicated that the presence of low levels of Cl^- can hinder the degradation of organic matter, due to the interaction between Cl^- and $SO_4^{\bullet-}$ as well as $^{\bullet}OH$, and resulting in the formation of RCSs with weak oxidizing properties [7]. Further, at a high Cl^- concentration, PMS can directly react with Cl^- to generate HClO, which exhibits a high selectivity towards organic matter. For organic matter containing electron-donating groups (such as, -OH, -NH_2, -R) can be easily oxidized by HClO, resulting in an increased degradation rate. However, the presence of electron withdrawing group (such as, -COOH, -NO_2), which reduces the electron density in a molecule, thereby reducing the reactivity with HClO, leading to a lower reaction rate [13]. The RhB contain both electron-donating groups (-R) and electron-withdrawing groups (-COOH), but the number of its electron-donating groups is more than that of electron-withdrawing groups, so the overall electron-donating group play a dominant role [31]. This property makes RhB highly reactive with HClO and therefore the k_{obs}

increased in high-chlorine systems. In addition, the effect of Cl^- concentration on RhB adsorption was monitored (S15), a slight decreasing trend from 2.46% to 0.14% of RhB removal. This may be due to the degree of aggregation of ionic dyes increase in the presence of Cl^-, which hinders the adsorption of RhB on the catalyst surface [31].

The TOC removal of RhB was measured and depicted in Fig. 1b, which similar trend of the decolorization. As the [Cl^-] increased from 0 to 5 mM, it was found that the TOC removal decreased from 39.64% to 23.45%. However, it gradually increased to 78.06% at 500 mM of [Cl^-]. It could be explained that under 5 mM [Cl^-], Cl^- reacted with $SO_4^{\bullet-}$ and $^{\bullet}OH$, then formed into less reactive RCSs ($Cl^{\bullet}$, $ClO^{\bullet}$, and $Cl_2^{\bullet-}$), resulting in the decline of the decolorization and mineralization. This process also generated refractory chlorination by-products, which hindered the deep mineralization [8]. With the increase of [Cl^-], more amount of HClO generated (Eqs. 5–6), which was beneficial for the thorough oxidation of the by-products [32].

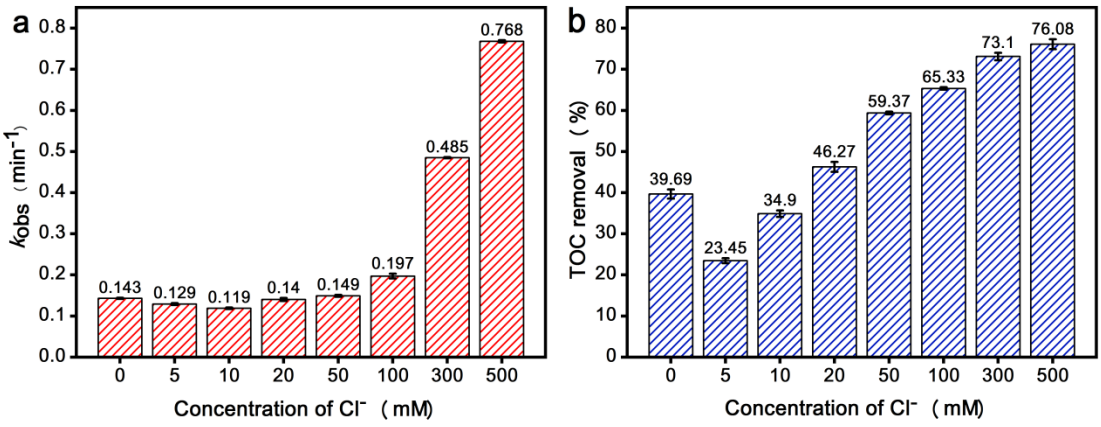

Fig. 1. Effects of Cl^- concentration on RhB removal (a) k_{obs} (b) TOC removal. Experiment conditions: $[RhB]_0$ = 20 mg/L, [PMS] = 1 mM, [Catalyst] = 20 mg/L, $[Cl^-]$ = 0–500 mM, 30 min, pH_i 6.4.

3.2 Roles of reactive species for the degradation of RhB

Previous studies have mostly employed kinetic modeling methods to investigate the impact of chloride ion concentration on ROSs and RCSs in the system, and lack of the direct experimental evidence [10, 13, 33, 34]. Herein, scavenging and EPR experiments were used to investigate the transformation of oxidizing species in Cl^- containing systems [35, 36]. To determine the dominant oxidizing species in the CoS@FeS/PMS system under different $[Cl^-]$, quenching experiments towards ROSs (eg., $O_2^{\bullet-}$, $^{\bullet}OH$, and $SO_4^{\bullet-}$ and $^1O_2$), as well as the possible coexisting RCSs (eg., $Cl^{\bullet}$, $Cl_2^{\bullet-}$ and HClO) were conducted. For MeOH, the rate constants with $SO_4^{\bullet-}$, $^{\bullet}OH$ and $Cl^{\bullet}$ are 2.5×10^7 $M^{-1}s^{-1}$, 9.7×10^8 $M^{-1}s^{-1}$ and 5.7×10^9 $M^{-1}s^{-1}$, respectively [37, 38]. For TBA, the reaction rate constants towards $^{\bullet}OH$, $Cl^{\bullet}$, and $Cl_2^{\bullet-}$ are 7.6×10^8 $M^{-1}s^{-1}$, 1.5×10^9 $M^{-1}s^{-1}$ and 7×10^2 $M^{-1}s^{-1}$ [39, 40], respectively, which can scavenge $^{\bullet}OH$ and $Cl^{\bullet}$, but with a negligible scavenging effect on $Cl_2^{\bullet-}$. Hence, if $SO_4^{\bullet-}$ is the main oxidant, the contribution of $SO_4^{\bullet-}$ can be qualitatively estimated from the distinction of the RhB removal between MeOH and TBA quenching tests. IPA can react with $^{\bullet}OH$, $Cl^{\bullet}$, and $Cl_2^{\bullet-}$, with their rate constants of 2.9×10^9 $M^{-1}s^{-1}$, 6×10^9 $M^{-1}s^{-1}$, and 1.2×10^5 $M^{-1}s^{-1}$ [41-43], respectively. Similarly, the contribution

of $Cl_2^{\bullet-}$ can be qualitatively estimated from the distinction of the RhB removal between the quenching by TBA and IPA [8]. FFA and L-histidine both showed high reactivity with $^1O_2$, with the reaction rates of 1.2×10^8 $M^{-1}s^{-1}$ and 3.2×10^7 $M^{-1}s^{-1}$, respectively [44, 45]. However, FFA or L-his is a reducing agent which may induce rapid PMS consumption, thus cannot identify the exact quenching effect towards $^1O_2$ [46-48]. Hence, the β-Carotene as a typical scavenger of $^1O_2$ (k = 2–3.0×10^{10} $M^{-1}s^{-1}$) is further introduced into the quenching tests to verify the contribution of $^1O_2$, since it is hardly oxidized by PMS [49]. For NH_4^+, it would hydrolyze into neutral amine, and react with HClO to form chloramines with much weaker oxidants [30, 50] (Eqs. 10–12), thus $(NH_4)_2SO_4$ was introduced as a scavenger to evaluate the contribution of HClO. To rule out the effect of SO_4^{2-}, same amount of Na_2SO_4 was added, and nearly no change on RhB removal (S16). Further, EPR experiments under different [Cl^-] were conducted to identify these reactive species. $SO_4^{\bullet-}$ and $^{\bullet}OH$ were trapped using DMPO as the spin trapping agent, while $Cl_2^{\bullet-}$ and $^1O_2$ were verified by employing PBN and TEMPO as the spin trapping agent [51]. The concentration of HClO was carried out by N, N-diethyl-p-phenylenediamine (DPD) method [8].

$$NH_3 + HClO \rightarrow HN_2Cl + H_2O \qquad k = 4.2 \times 10^6\ M^{-1}s^{-1} \qquad (10)$$

$$NH_2Cl + HClO \rightarrow HNCl_2 + H_2O \qquad k = 3.5 \times 10^2\ M^{-1}s^{-1} \qquad (11)$$

$$HNCl_2 + HClO \rightarrow NCl_3 + H_2O \qquad k = 2.1\ M^{-1}s^{-1} \qquad (12)$$

As show in Fig. 2a–c, in the absence of Cl^-, the RhB removal decreased from 98.68% to 77.10% and 58.02%, when MeOH and β-Carotene added separately. Under

low [Cl^-] of 5 mM, the addition of MeOH, IPA and β-Carotene affected on the removal of RhB, decreased from 98.07% to 77.88%, 72.90% and 51.03%, respectively. This results demonstrate that the previously dominant reactive species of $^1O_2$, $SO_4^{\bullet-}$ were gradually converted into $^1O_2$, $SO_4^{\bullet-}$ and $Cl_2^{\bullet-}$, when the [Cl^-] increased from 0 to 5 mM. Under high [Cl^-] of 500 mM, when MeOH, IPA, β-Carotene and $(NH_4)_2SO_4$ were separately added, the RhB removal decreased from 89.99% to 88.64%, 70.89%, 79.14% and 23.4% within 3 min, respectively, implies that the primary oxidizing species were HClO, accompanying with a certain amount of $Cl_2^{\bullet-}$ and $^1O_2$. Interestingly, it is observed that $Cl_2^{\bullet-}$ concentration increases as the Cl^- concentration increases (Fig 3e), while the quenching results showed that the contribution of $Cl_2^{\bullet-}$ was no significant change. This may be attributed to the low oxidation capacity of $Cl_2^{\bullet-}$. Moreover, in high concentration Cl^- systems, a substantial amount of HClO was generated through the direct reaction between Cl^- and PMS, and then rapid oxidation of RhB. Therefore, the contribution of $Cl_2^{\bullet-}$ to the degradation of RhB was not significantly improved.

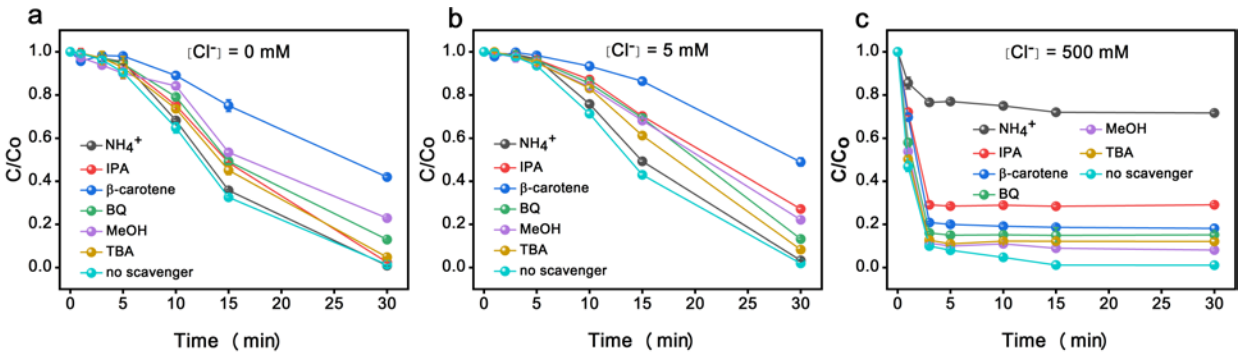

Fig. 2. Effect of [Cl^-] on reactive species for the degradation of RhB. Experiment conditions: (a-c) [Catalyst] = 20 mg/L; $[RhB]_0$ = 20 mg/L, [PMS] = 1 mM; (a) [Cl^-] = 0 mM; (b) [Cl^-] = 5 mM; (c) [Cl^-] = 500 mM.

3.3 Transformation between ROSs and RCSs

We further amplified the variation process of the contribution of $SO_4^{\bullet-}$, $^{\bullet}OH$ and $^1O_2$ under 0, 5, 10, 20, 50, 100, 300 and 500 mM Cl^-, using 1 M of MeOH and 0.5 mM of β-Carotene as scavengers individually, to exactly describe the variation trend. Their quenching contribution to each entry was calculated by the RhB removal differences, as detailed in Table S17–18. As depicted in Fig. 3a, the inhibitory effect towards $SO_4^{\bullet-}$ and $^{\bullet}OH$ gradually decreased with the increasing [Cl^-]. This tendency was further verified by the EPR capturing results (Fig. 3b), which showed the same decreasing intensities of the $SO_4^{\bullet-}$ and $^{\bullet}OH$ signal peaks, even completely disappeared under 500 mM. In contrast, the $Cl_2^{\bullet-}$ signal peaks gradually increased and became very strong at 500 mM (Fig. 3e) [8, 52], indicating that high [Cl^-] prompted the conversion of $SO_4^{\bullet-}$ and $^{\bullet}OH$ into RCSs, resulting in the formation of $Cl_2^{\bullet-}$ with weaker reactivity.

The inhibition effect of β-Carotene towards $^1O_2$ showed a parabolic tendency as [Cl^-] increased, which enhanced between 0–10 mM and then decreased between 20–500 mM (Fig. 3c). This phenomenon was also consistent with the variation trend of the $^1O_2$ EPR signal peaks, which enhanced obviously with 5 mM of Cl^-, and weaken

between 20–500 mM of Cl^- (Fig. 3d). This may be due to that the consumption of Cl^- on $SO_4^{\bullet-}$ and $^{\bullet}OH$ accelerates the PMS decomposition, and produces more $^1O_2$ (Eq. 13) [31]. In addition, $^1O_2$ could be efficiently generated through the interaction between HSO_5^- and Cl_2 [53] (Eqs. 14–15), with a reaction rate constant of 1.5×10^5 $M^{-1}s^{-1}$. However, under high [Cl^-] (500mM), more Cl^- reacted with HSO_5^- and formed abundant HClO, thus inhibiting the decomposition of HSO_5^- to generate $^1O_2$, as well as the pathway through Cl_2. Besides, due to the abundant Cl^- were easily blocked the active sulfur vacancies, which was responsible for the adsorption of dissolved O_2 and later conversion into $^1O_2$, thus shrinked the generation of $^1O_2$. (Eqs. 16–17). To convince this point, we analyzed the concentrations of the accompanying H_2O_2 under various [Cl^-] systems (Eq. 17, see Fig. 3f). It was found that when the [Cl^-] increased from 0 to 500 mM, the concentration of H_2O_2 decreased by 42.2%, which verified the above assumption. Furthermore, the concentrations of HClO were monitored under different [Cl^-] (Fig. 5b), a straight upward trend was observed, with the [Cl^-] increased from 50 mM to 500 mM, the HClO concentration increased from 1.29 mg/L to 13.81 mg/L in the CoS@FeS/PMS system.

$$HSO_5^- + SO_5^{2-} \rightarrow HSO_4^- + SO_4^{2-} + {}^1O_2 \quad (13)$$

$$HClO + 2H^+ + Cl^- \rightarrow Cl_2 + H_2O \quad (14)$$

$$Cl_2 + HSO_5^- + H_2O \rightarrow {}^1O_2 + SO_4^{2-} + 2Cl^- + 3H^+ \quad (15)$$

$$O_2 + e^- \rightarrow O_2^{\bullet-} \quad (16)$$

$$2O_2^{\bullet-} + 2H^+ \rightarrow {}^1O_2 + H_2O_2 \quad (17)$$

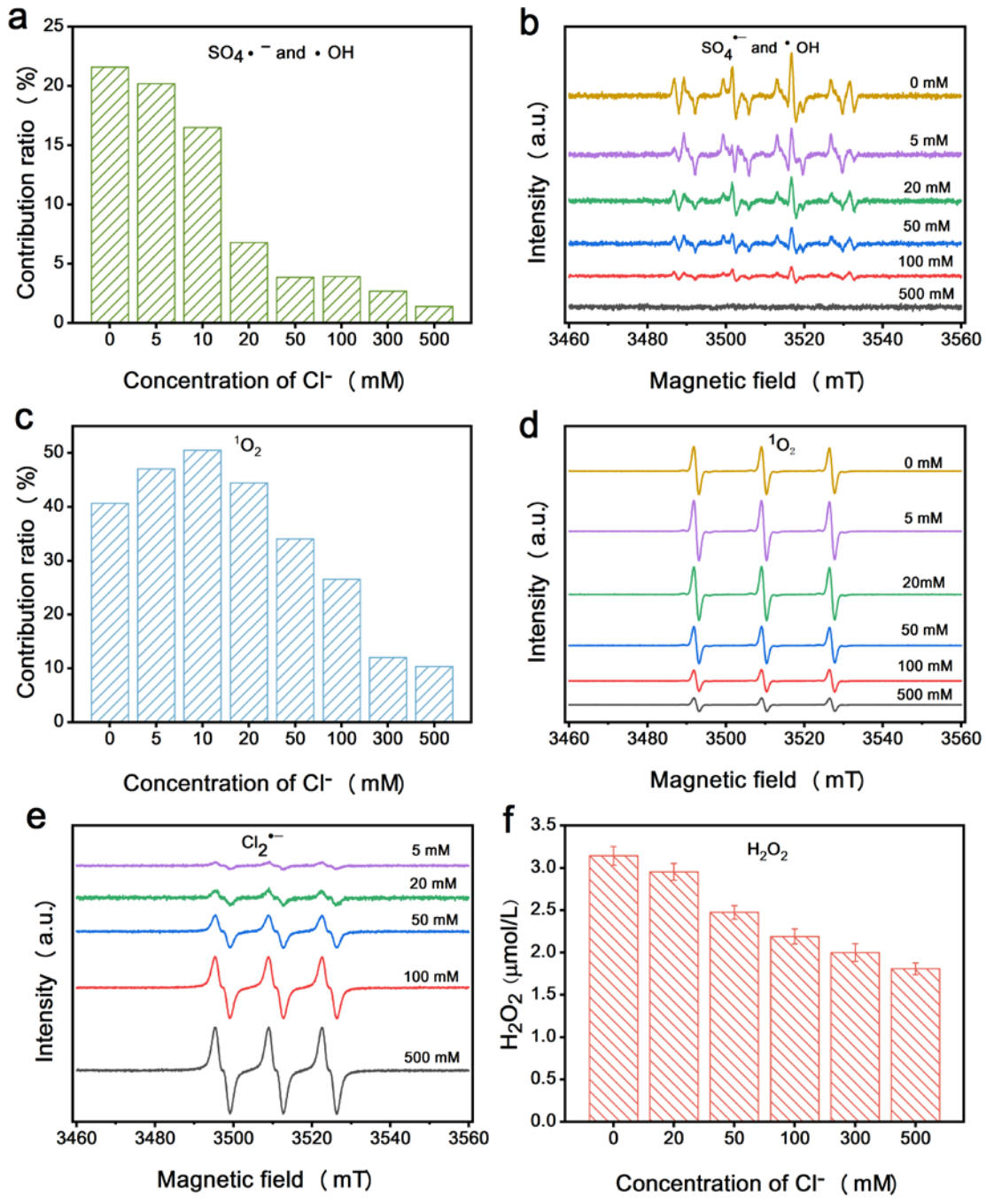

307

308 **Fig. 3.** Effect of [Cl^-] on the generation and transformation of reactive

309 oxidative species. Experiment conditions: (a-f) [Catalyst] = 20 mg/L, [Cl^-]

310 = 0–500 mM; (a-e) [PMS] = 1 mM; (a,c) $[RhB]_0$ = 20 mg/L.

311

To enhance the validity of our experimental results, we conducted molecular probe experiments to assess the impact of Cl^- concentration on the steady-state concentration of reactive oxygen species and their corresponding contribution [23, 54]. In view of the quenching and EPR experiments of the CoS@FeS/PMS/Cl^- system as discussed above, the degradation of RhB can be attributable to $SO_4^{\bullet-}$, $^{\bullet}OH$, $^1O_2$, RCSs, and HClO (Eq. 18). The relative contributions of RhB degradation by $SO_4^{\bullet-}$, $^{\bullet}OH$, $^1O_2$, RCSs, and HClO can thus be expressed by Eqs. 19–22.

$$-\ln\frac{[RhB]}{[RhB]_0} = k_{RhB,\ SO_4^{\bullet-}}[SO_4^{\bullet-}]_{ss} + k_{RhB,\ ^{\bullet}OH}[^{\bullet}OH]_{ss} + k_{RhB,\ ^1O_2}[^1O_2]_{ss} + k'_{RCSs,HClO} \quad (18)$$

where $k_{RhB,SO_4^{\bullet-}}$, $k_{RhB,^{\bullet}OH}$ and $k_{RhB,^1O_2}$ are the second order rate constants for the reaction of RhB with $SO_4^{\bullet-}$, $^{\bullet}OH$ and $^1O_2$. The $k'_{RCSs,HClO}$ represents the contribution of RCSs and HClO to RhB degradation.

$$f_{SO_4^{\bullet-}} = \frac{k_{RhB,\ SO_4^{\bullet-}}[SO_4^{\bullet-}]_{ss}}{-\ln\frac{[RhB]}{[RhB]_0}} \quad (19)$$

$$f_{^{\bullet}OH} = \frac{k_{RhB,\ ^{\bullet}OH}[^{\bullet}OH]_{ss}}{-\ln\frac{[RhB]}{[RhB]_0}} \quad (20)$$

$$f_{^1O_2} = \frac{k_{RhB,\ ^1O_2}[^1O_2]_{ss}}{-\ln\frac{[RhB]}{[RhB]_0}} \quad (21)$$

$$f_{RCSs,HClO} = 1 - f_{SO_4^{\bullet-}} - f_{^{\bullet}OH} - f_{^1O_2} \quad (22)$$

where $f_{SO_4^{\bullet-}}$, $f_{\bullet OH}$, $f\ ^1O_2$, and $f_{RCSs,HClO}$ are the contributions ration of RhB degradation by $SO_4^{\bullet-}$, $^{\bullet}OH$, $^1O_2$, RCSs, and HClO.

The steady-state concentration of $SO_4^{\bullet-}$, $^{\bullet}OH$ and $^1O_2$ were shown in Fig 4a–c. As the Cl^- concentration increased from 0 to 500 mM, the steady-state concentrations of $SO_4^{\bullet-}$ and $^{\bullet}OH$ decreased from 1.8 $\times 10^{-10}$ M s and 1.48$\times 10^{-10}$ M s to 0.35 $\times 10^{-10}$ M s and 0.23 $\times 10^{-10}$ M s, respectively. Similarly, the contribution of $SO_4^{\bullet-}$, $^{\bullet}OH$ to the RhB removal decreased from 28.1% and 14.1% to 1.7% and 0.4% (Fig. 4d). The steady-state concentration and contribution of $^1O_2$ exhibited a parabolic curve. With an increase in Cl^- concentration, the steady-state concentration of $^1O_2$ initially showed a slight increase from 0.72 $\times$ 10^{-8} M s to 0.74 $\times$ 10^{-8} M s, followed by a rapid decrease to 0.21 $\times$ 10^{-8} M s. In parallel, the contribution of $^1O_2$ increased from 52.8% to 60.7% and eventually decreased to 2.8%. On the other hand, the contribution of HClO and RCSs sharply increased from 5.1% to 95.0% with the increase of Cl^- concentration. These findings were consistent with the quenching experimental and EPR results.

Based on the above experimental results, with an increase in Cl^- concentration, the concentration of $SO_4^{\bullet-}$, $^{\bullet}OH$, as well as their contribution to the degradation of RhB, gradually decreased. $^1O_2$ exhibited a dual trend, initially increasing and then decreasing, whereas HClO and RCSs showed an increasing trend.

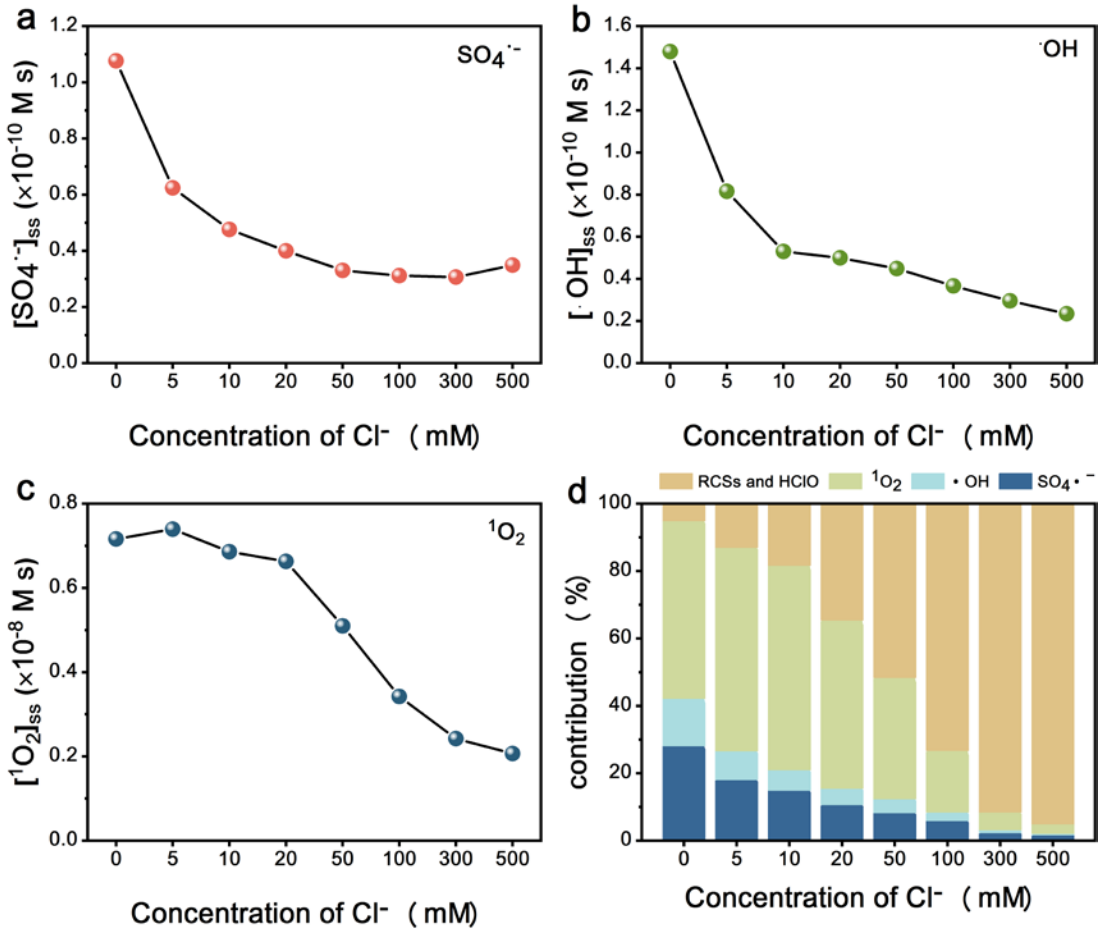

Fig. 4. The steady-state concentration and contribution of reactive oxygen species. Experiment conditions: (a-d) [Catalyst] = 20 mg/L, [PMS] = 1 mM, $[RhB]_0$ = 20 mg/L, $[Cl^-]$ = 0–500 mM.

3.3 The role of catalyst

3.3.1 AOX formation

In the presence of Cl^-, numerous chlorinated byproducts were formed due to the RCSs and HClO (Eqs. 23–24) [55], which results into the formation of abundant AOX. As shown in Fig. 5a, the AOX concentrations under different $[Cl^-]$ were detected, which increased from 0.067 to 0.457 mg/L with the enhancement of $[Cl^-]$

from 50 to 500 mM. While the addition of catalysts can significantly reduce the amount of AOX generated in the system, especially under high [Cl^-] of 300 mM and 500 mM, the concentration of AOX reduce 56.45% and 43.03%, respectively. In addition, compared with the PMS/Cl^- system, the CoS@FeS/PMS/Cl^- system showed a reduction of 20.4% and 25.1% in AOX concentrations produced by SMX and BPA, respectively. This indicates the versatility of the catalyst in inhibiting AOX formation (S19). Since HClO were estimated to be the dominant oxidants at 500 mM [Cl^-], the corresponding HClO concentrations were further determined. It was found that the HClO concentration increased as the [Cl^-] increased, and the addition of catalysts could obviously reduce the amount of HClO, the decreasement became more obvious with the increasing [Cl^-]. For instance, the HClO concentration decreased from 24.24 to 13.81 mg/L as the catalyst dosage increases from 0 to 20 mg/L, under 500 mM [Cl^-] (Fig. 5b). On the one hand, the catalyst CoS@FeS could compete with Cl^- to react with HSO_5^-, which may impact the generation of HClO. On the other hand, our previous studies have revealed that CoS@FeS has an abundance of sulfur vacancies (SVs) on catalyst surface, which availed the adsorption of O_2 and consequently produce $^1O_2$ along with H_2O_2 (Eqs. 16–17) [21]. Interestingly, literatures have reported that in-situ electrochemical synthesis or ex-situ addition of H_2O_2 could react with HClO (Eq.25), and minimize chlorinated disinfection by-products (Cl-DBPs) [56-60]. Based on this understanding, we hypothesize that the in-situ generation of H_2O_2 on the catalyst surface might lead to the consumption of

HClO, ultimately leading to a decrease in AOX concentration. To validate this hypothesis, we conducted a series of comprehensive verification experiments.

$$R^{\bullet} + Cl_2^{\bullet -} \rightarrow RCl + Cl^- \quad (23)$$

$$RH + HClO \rightarrow RCl + H_2O \quad (24)$$

$$H_2O_2 + HClO \rightarrow H^+ + Cl^- + H_2O + {}^1O_2 \quad (25)$$

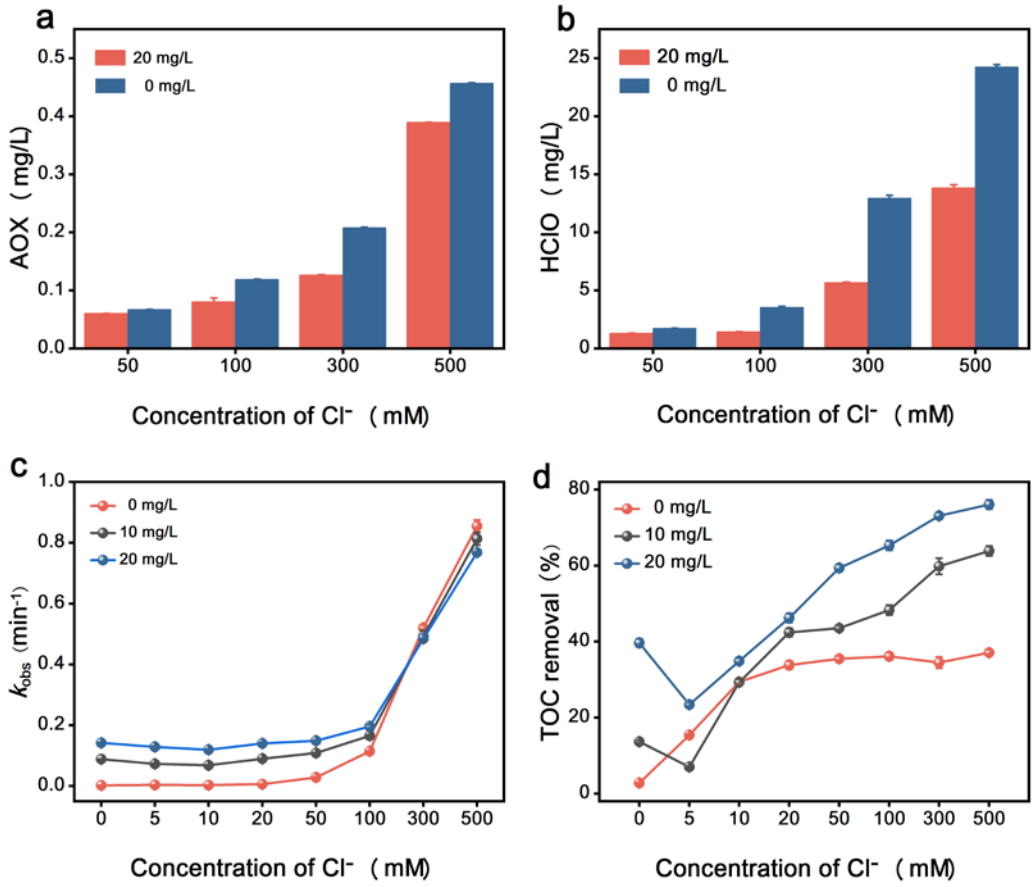

Fig. 5. Effect of catalyst dose on (a) AOX concentration, (b) HClO concentration, (c) degradation rate, and (d) mineralization of RhB. Experimental conditions: (a–d) $[RhB]_0$ = 20 mg/L, [PMS] = 1 mM, [Catalyst] = 0–20 mg/L, $[Cl^-]$ = 0–500 mM.

The concentration of in-situ generated H_2O_2 in the CoS@FeS system with different catalyst dosages were measured (Fig. 6a). Results showed that the

concentration of H_2O_2 in solution increased from 0.14 μmol/L to 9.43 μmol/L (in 80 min), with the catalyst dosage increased from 0 to 100 mg/L. To further confirm the origin of the in-situ generation of H_2O_2 on the surface of CoS@FeS, we tested the H_2O_2 concentration under O_2/air/N_2 atmosphere in 40 mg/L CoS@FeS solution (Fig. 6b). As expected, the amount of the generated H_2O_2 decreased obviously when the O_2 concentration declined. When under O_2 atmosphere, the amount of H_2O_2 was 1.96/4.73 times of in air or nitrogen at 80 minutes. It revealed the O_2 concentration related closely with the in-situ generation of H_2O_2. Moreover, the results show that the concentration of HClO decreased gradually as the amount of catalyst in the PMS/Cl^- system increased (Fig. 6c). Specifically, when the catalyst dosage was increased from 0 to 100 mg/L, the concentration of HClO decreased from 24.24 mg/L to 2.4 mg/L, which represents a decrease of 10.1 times. The experimental results presented above demonstrate that the interaction between catalyst and O_2 leads to the formation of H_2O_2, which can impede the production of HClO.

Next, to highlight the crucial role of SVs on the catalyst's surface in H_2O_2 production, we conducted a modification of the catalyst using $NaBH_4$, resulting in varying amounts of SVs. The catalysts modified by $NaBH_4$ at concentrations of 0, 0.05, and 0.1 mM were named as CoS@FeS-1, CoS@FeS-2, and CoS@FeS-3, respectively. The EPR spectra of SVs results revealed a gradual increase in the number of SVs on the catalyst's surface with the increase in $NaBH_4$ concentration (Fig. 6d). And the concentrations of $^1O_2$ (S20) and H_2O_2 (Fig. 6e) exhibited

significant increases, which demonstrated the crucial role of SVs for the production of H_2O_2. In particular, as the concentration of in-situ H_2O_2 production increased from 1.24 to 2.14 μmol/L within 20 min, the concentration of HClO and AOX in the chlorine-containing system decreased by 68.2% and 50.6%, respectively (Fig. 6f, g).

To further demonstrate the important role of H_2O_2 in inhibiting AOX, we observed the changes in HClO and AOX by prolonging the contact time of the catalyst with O_2 and accumulating the in-situ production of H_2O_2. The results indicate that as the dosing time of the catalyst increases from 0 to 60 min, the accumulation of H_2O_2 increases from 0.19 to 2.65 μmol/L (Fig. 6a). In parallel, the HClO concentration decreases from 13.81 to 6.39 mg/L, and the AOX concentration decreases significantly from 0.389 to 0.232 mg/L (Fig. 6h, i). Furthermore, to intuitively demonstrate the effect of H_2O_2 on inhibiting the formation of AOX, we directly added H_2O_2 to the CoS@FeS/PMS/Cl^- system and monitored its impact on HClO and AOX. As the concentration of H_2O_2 increased, the content of HClO decreased significantly (S21a). At a H_2O_2 dose of 1 mM, the AOX concentration dropped to 0.026 mg/L (S21b).

Above all, it could be concluded that the sulfur vacancies adsorbed O_2, via $O_2^{\bullet-}$ and converted into $^1O_2$, simultaneously in-situ produced H_2O_2, then quickly reacted with the formed HClO（Eq. 25）, thus decreased the AOX concentration. This process may provide a potential strategy for reducing

the high levels of AOX and toxicity during the PMS oxidation in environments under high [Cl^-].

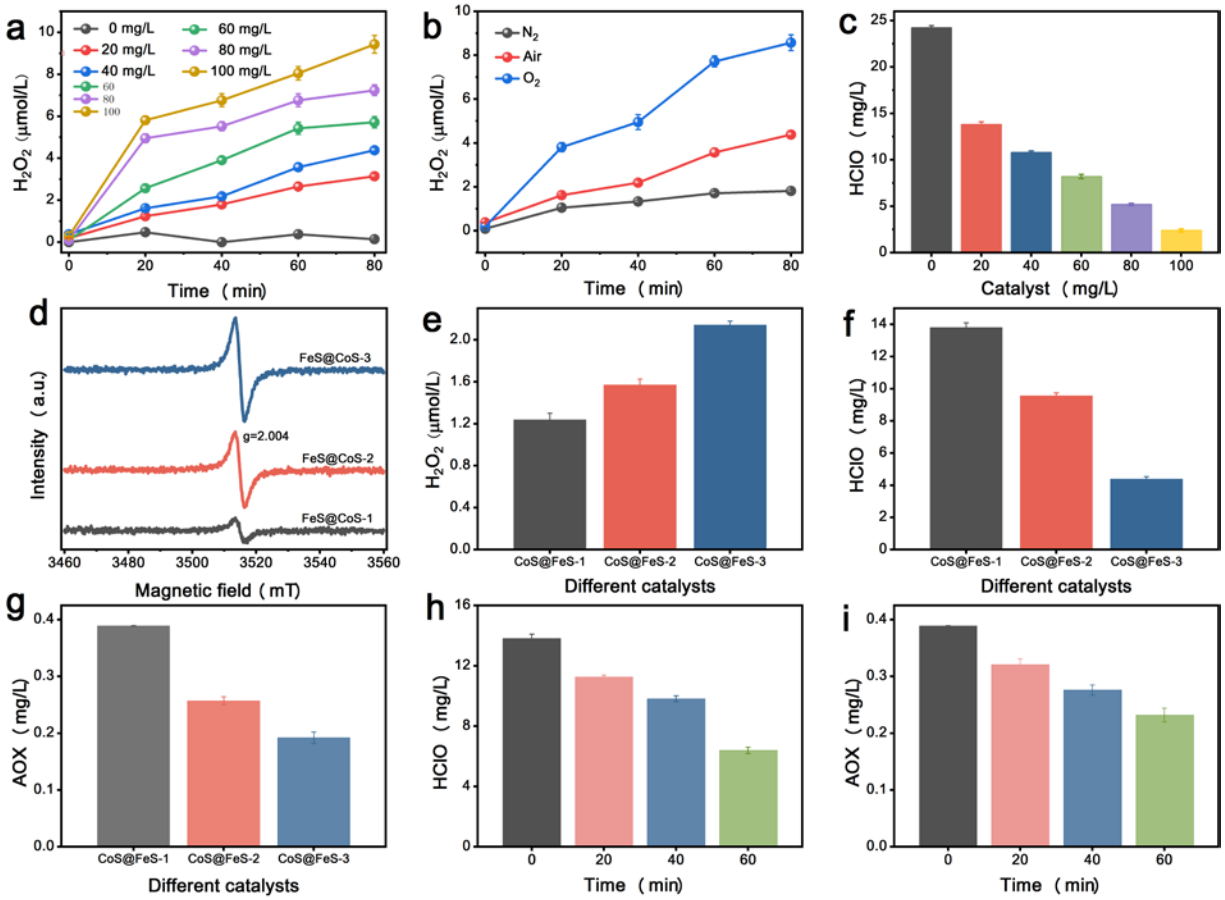

Fig. 6. Concentration of HClO and H_2O_2 detected. Experimental conditions: (a, c) [Catalyst] = 0–100 mg/L, (b) [Catalyst] = 40 mg/L, (d–i) [Catalyst] = 20 mg/L; (a–c, e–i) [Cl^-] = 500 mM, (c-i) [PMS] = 1 mM; (g, i) $[RhB]_0$ = 20 mg/L.

3.3.2 Degradation rate

To clarify the contribution of CoS@FeS, the RhB removal under different catalyst dosages, in the presence of 0–500 mM [Cl^-], were comparatively studied, as shown in Fig.5c. It was observed that increasing the catalyst dose had a noticeable advantageous impact on the degradation rate of RhB at low [Cl^-] (0–50

mM) (Fig. 3a). However, this effect became limited when the Cl^- concentration was high (100–500 mM). For instance, when the catalyst dose was increased from 0 to 20 mg/L, the degradation rate of RhB increased significantly from 0.004 to 0.073 min^{-1} at 5 mM [Cl^-]. Under 500 mM [Cl^-], the k_{obs} decreased slightly from 0.855 to 0.768 min^{-1}, indicated the ineffectiveness of the catalyst and the importance of HClO. Quenching and EPR experiments revealed that under low [Cl^-] (5 mM), the main reactive oxygen species are $SO_4^{\bullet-}$, $^{\bullet}OH$ and $^1O_2$. Increasing the amount of catalyst dosage provides more active sites to generate ROSs, thus improved the degradation rate. Under a high concentration of Cl^- ([Cl^-] = 500 mM), HClO becomes the main oxidizing substance in both the PMS/Cl^- and CoS@FeS/PMS/Cl^- systems. The presence of a catalyst reduces the amount of HClO in the system (Fig.5b), resulting in lower k_{obs} of RhB. Furthermore, in the PMS/Cl^- system, the degradation rate of RhB increases gradually as the concentration of Cl^- increases. This is mainly because without the addition of catalysts, the oxidants in the system are only HClO [32], which depends on the Cl^- concentrations [14].

3.3.3 Mineralization

Previous studies indicated the complete removal of organic contaminants in AOPs may not represent the overall mineralization [61]. In Fig. 5d, it can be observed that without catalyst, the TOC removal increased with the [Cl^-], until it reaches approximately 36% and remains at this level. However, in the presence of the catalyst, the mineralization decreased slightly from 0–5

453 mM [Cl^-], but showed higher TOC removal for the entire [Cl^-] range of 5–
454 500 mM. The main reasons could be that the catalyst significantly inhibits the
455 formation of AOX in saline systems, which are often toxic and difficult to degrade
456 further. Earlier studies reported that the short-chain carboxylic acid
457 intermediates are responsible for the excessive TOC in the reaction system
458 [62]. Herein, the HPLC-MS method was used to analyze the RhB
459 intermediates in the PMS/Cl^- system and found a large number of organic
460 acids (S22), which was consistent with these findings [50]. As the only
461 oxidizing substance in the PMS/Cl^- system was HClO, which has low
462 reactivity with a carboxylic acid organic compound [13], thus caused
463 insufficient mineralization of RhB. In the presence of the catalyst, the
464 formed $^1O_2$ enables further oxidative degradation of these intermediates.
465 Despite no significant signal peaks of $SO_4^{\bullet-}$ and $^{\bullet}OH$ could be observed in
466 the EPR capturing spectrum, which may be due to the low concentration
467 level and fast decomposition rates under high Cl^- conditions [63],
468 quenching tests revealed a little amount existence of the two species. $SO_4^{\bullet-}$
469 is electrophilic, and is very easy to react with the electron-donating groups (–NH_2,
470 –R) on the RhB, thereby destroying the RhB. In addition, $SO_4^{\bullet-}$ is very oxidative
471 with a redox potential of 2.6–3.1 V, which favors the opening of the benzene ring.
472 Undoubtedly, $SO_4^{\bullet-}$ and $^{\bullet}OH$ still worked in the mineralization of RhB and

its intermediates. Therefore, the addition of the catalysts under high chlorine conditions can significantly increase the mineralization of RhB.

3.4 Intermediates and toxicity assessment

HPLC-MS was employed to analyze the degradation products of RhB under different Cl^- concentrations and propose potential degradation pathways. Initially, the degradation pathway of RhB was examined in the absence of Cl^-. Combined with the results of HPLC-MS and existing literature [14, 22, 64], three possible paths for RhB degradation were proposed, namely deethylation, carbon-carbon bond rupture and hydroxylation (S23 a). Moreover, the experimental results revealed the presence of various chlorinated by-products in the chlorine-containing systems, including CoS@FeS/ PMS/Cl^- ([Cl^-] = 5 mM), CoS@FeS/PMS/Cl^- ([Cl^-] = 500 mM), and PMS/Cl^- ([Cl^-] = 500 mM) systems (S23 b–e). This can be attributed to the addition of RCSs and HClO to RhB and its intermediates, leading to the formation of chlorinated by-products. Additionally, it was observed that the degradation products and pathways of RhB in CoS@FeS/PMS/Cl^- ([Cl^-] = 500 mM) and PMS/Cl^- ([Cl^-] = 500 mM) systems were similar (S23 c–d), indicating that the primary reactive oxygen species in the high-concentration Cl^- system was HClO.

The toxicity of RhB and its intermediates can be evaluated using luminescent bacteria assays, where higher luminescence inhibition indicates greater acute toxicity [11]. When Cl^- was absent, the luminescence inhibition of the RhB solution was

493 28.3%. However, when the solution contained a Cl^- concentration of 500 mM, the
494 luminescence inhibition significantly increased to 76.8%. This rise in toxicity can be
495 attributed to the low steric hindrance of the chlorinated byproduct, which allows it to
496 easily penetrate the luminescent bacteria [65]. As a result, the acute toxicity of the
497 solution escalates. According to our study, the introduction of a catalyst has been
498 found to decrease the concentration of AOX (Fig. 5a). In order to investigate whether
499 the catalyst can also reduce the acute toxicity of the reaction solution, we conducted
500 toxicity measurements on the PMS/Cl^- system (Fig 7). The results revealed that the
501 luminescence inhibition of PMS/Cl^- reached 98.7% when the Cl^- concentration was
502 500 mM, which was significantly higher than that of the CoS@FeS/PMS/Cl^- system.
503 Therefore, the inclusion of catalysts effectively reduces the acute toxicity of
504 chlorine-containing systems by lowering AOX concentrations.

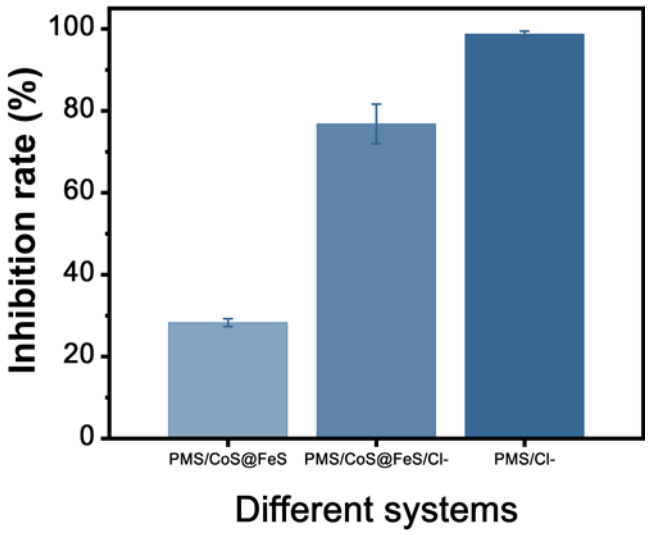

505

Fig.7. Acute biotoxicity assays of RhB in different systems. Experimental conditions: [Catalyst] = 0–20 mg/L, [PMS] = 1 mM, $[RhB]_0$ = 20 mg/L, $[Cl^-]$ = 0–500 mM.

4 Conclusions

The treatment of organic contaminants in high Cl^- wastewater using PMS activation poses a challenge. In this study, we thoroughly investigated the impact of Cl^- on PMS activation and proposed a new mechanism to prevent the formation of AOX. Our research found that the CoS@FeS/PMS catalyst exhibited a dual effect on RhB removal, with low-concentration inhibition and high-concentration promotion. EPR capturing, quenching tests, and molecular probe experiments demonstrate that the concentration of Cl^- has a significant impact on the conversion of oxidative species. During exploration of the role of catalysts, we discovered that they not only improve RhB mineralization but also inhibit AOX. It could be concluded that the sulfur vacancies adsorbed O_2, via $O_2^{\bullet -}$ and converted into $^1O_2$, simultaneously in-situ produced H_2O_2, quickly reacted with the formed HClO, thus decreased the AOX concentration. Therefore, our study provides new insights into the underlying mechanism of the $^1O_2$-dominated system to inhibit the accumulation of AOX.

CRediT authorship contribution statement

Liyuan Wu: Conceptualization, Writing – review & editing, Supervision, Funding acquisition; **Chenjing Hou:** Investigation, Methodology, Formal analysis, Data curation, Writing – original draft; **Xin Wang:** Software; **Pengpeng Guo:** Data curation; **Xiaoran Zhang:** Resources; **Yi Jin:** Resources; **Yongwei Gong:** Resources; **Xudan Chen:** Software; **Haiyan Li:** Reviewing.

Declaration of Competing Interest

The authors declare that they have no known competing financial interests or personal relationships that could have appeared to influence the work reported in this paper.

Acknowledgements

This work was supported by the National Natural Science Foundation of China (No. 52100001 and 51978032); the Youth Top Talents Training Program of the Beijing Municipal Education Commission (CIT&TCD201804052), the Youth Beijing Scholars program (No. 024), The Graduate Innovation Program of Beijing University of Civil Engineering and Architecture (PG2023069).

Appendix A. Supplementary data

Supplementary data to this article can be found online.

References

[1] S. Giannakis, K.-Y.A. Lin, F. Ghanbari, A review of the recent advances on the

544 treatment of industrial wastewaters by Sulfate Radical-based Advanced Oxidation
545 Processes (SR-AOPs), Chemical Engineering Journal 406 (2021) 127083.
546 [2] N. Li, Y. Wang, X. Cheng, H. Dai, B. Yan, G. Chen, L. Hou, S. Wang, Influences
547 and mechanisms of phosphate ions onto persulfate activation and organic degradation
548 in water treatment: A review, Water Res 222 (2022) 118896.
549 [3] L. Lian, B. Yao, S. Hou, J. Fang, S. Yan, W. Song, Kinetic Study of Hydroxyl and
550 Sulfate Radical-Mediated Oxidation of Pharmaceuticals in Wastewater Effluents,
551 Environ Sci Technol 51 (2017) 2954-2962.
552 [4] Y. Wang, Y. Sun, R. Wang, M. Gao, Y. Xin, G. Zhang, P. Xu, D. Ma, Activation of
553 peroxymonosulfate with cobalt embedded in layered delta-MnO_2 for degradation of
554 dimethyl phthalate: Mechanisms, degradation pathway, and DFT calculation, J Hazard
555 Mater 451 (2023) 130901.
556 [5] Y. Wang, F. Gong, L. Diao, H. Liu, C. Hu, Y. Xin, D. Ma, Unveiling a
557 MnxCo1−xSe Fenton-like catalyst for organic pollutant degradation: A key role of
558 ternary redox cycle and Se vacancy, Separation and Purification Technology 294
559 (2022) 121196.
560 [6] H. Yi, Y. Wang, L. Diao, Y. Xin, C. Chai, D. Cui, D. Ma, Ultrasonic treatment
561 enhances the formation of oxygen vacancies and trivalent manganese on alpha-MnO_2
562 surfaces: Mechanism and application, J Colloid Interface Sci 626 (2022) 629-638.
563 [7] J. Peng, Z. Wang, S. Wang, J. Liu, Y. Zhang, B. Wang, Z. Gong, M. Wang, H.
564 Dong, J. Shi, H. Liu, G. Yan, G. Liu, S. Gao, Z. Cao, Enhanced removal of

methylparaben mediated by cobalt/carbon nanotubes (Co/CNTs) activated peroxymonosulfate in chloride-containing water: Reaction kinetics, mechanisms and pathways, Chemical Engineering Journal 409 (2021) 128176.

[8] C.-X. Chen, S.-S. Yang, J. Ding, G.-Y. Wang, L. Zhong, S.-Y. Zhao, Y.-N. Zang, J.-Q. Jiang, L. Ding, Y. Zhao, L.-M. Liu, N.-Q. Ren, Non-covalent self-assembly synthesis of AQ2S@rGO nanocomposite for the degradation of sulfadiazine under solar irradiation: The indispensable effect of chloride, Applied Catalysis B: Environmental 298 (2021) 120495.

[9] F. Yang, Y. Huang, C. Fang, Y. Xue, L. Ai, J. Liu, Z. Wang, Peroxymonosulfate/base process in saline wastewater treatment: The fight between alkalinity and chloride ions, Chemosphere 199 (2018) 84-88.

[10] Y. Huang, M. Jiang, S. Gao, W. Wang, Z. Liu, R. Yuan, Non-radical pathway dominated by singlet oxygen under high salinity condition towards efficient degradation of organic pollutants and inhibition of AOX formation, Separation and Purification Technology 291 (2022) 120921.

[11] C. Fang, D. Xiao, W. Liu, X. Lou, J. Zhou, Z. Wang, J. Liu, Enhanced AOX accumulation and aquatic toxicity during 2,4,6-trichlorophenol degradation in a Co(II)/peroxymonosulfate/Cl^- system, Chemosphere 144 (2016) 2415-2420.

[12] B. Sheng, Y. Huang, Z. Wang, F. Yang, L. Ai, J. Liu, On peroxymonosulfate-based treatment of saline wastewater: when phosphate and chloride co-exist, RSC Adv 8 (2018) 13865-13870.

586 [13] Y. Huang, B. Sheng, Z. Wang, Q. Liu, R. Yuan, D. Xiao, J. Liu, Deciphering the
587 degradation/chlorination mechanisms of maleic acid in the Fe(II)/peroxymonosulfate
588 process: An often overlooked effect of chloride, Water Res 145 (2018) 453-463.
589 [14] R. Yuan, S.N. Ramjaun, Z. Wang, J. Liu, Effects of chloride ion on degradation
590 of Acid Orange 7 by sulfate radical-based advanced oxidation process: implications
591 for formation of chlorinated aromatic compounds, J Hazard Mater 196 (2011)
592 173-179.
593 [15] R. Luo, M. Li, C. Wang, M. Zhang, M.A. Nasir Khan, X. Sun, J. Shen, W. Han, L.
594 Wang, J. Li, Singlet oxygen-dominated non-radical oxidation process for efficient
595 degradation of bisphenol A under high salinity condition, Water Res 148 (2019)
596 416-424.
597 [16] L. Kong, G. Fang, X. Xi, Y. Wen, Y. Chen, M. Xie, F. Zhu, D. Zhou, J. Zhan, A
598 novel peroxymonosulfate activation process by periclase for efficient singlet
599 oxygen-mediated degradation of organic pollutants, Chemical Engineering Journal
600 403 (2021).
601 [17] S. Wang, J. Tian, Q. Wang, F. Xiao, S. Gao, W. Shi, F. Cui, Development of CuO
602 coated ceramic hollow fiber membrane for peroxymonosulfate activation: a highly
603 efficient singlet oxygen-dominated oxidation process for bisphenol a degradation,
604 Applied Catalysis B: Environmental 256 (2019) 126445.
605 [18] P. Sun, H. Liu, M. Feng, L. Guo, Z. Zhai, Y. Fang, X. Zhang, V.K. Sharma,
606 Nitrogen-sulfur co-doped industrial graphene as an efficient peroxymonosulfate

activator: Singlet oxygen-dominated catalytic degradation of organic contaminants, Applied Catalysis B: Environmental 251 (2019) 335-345.

[19] Y. Gao, Y. Zhu, L. Lyu, Q. Zeng, X. Xing, C. Hu, Electronic Structure Modulation of Graphitic Carbon Nitride by Oxygen Doping for Enhanced Catalytic Degradation of Organic Pollutants through Peroxymonosulfate Activation, Environ Sci Technol 52 (2018) 14371-14380.

[20] S. Horikoshi, T. Miura, M. Kajitani, H. Hidaka, N. Serpone, A FT-IR (DRIFT) study of the influence of halogen substituents on the TiO2-assisted photooxidation of phenol and p-halophenols under weak room light irradiance, Journal of Photochemistry and Photobiology A: Chemistry 194 (2008) 189-199.

[21] L. Wu, P. Guo, X. Wang, H. Li, X. Zhang, K. Chen, P. Zhou, The synergy of sulfur vacancies and heterostructure on CoS@FeS nanosheets for boosting the peroxymonosulfate activation, Chemical Engineering Journal 446 (2022) 136759.

[22] J. Chen, L. Zhang, T. Huang, W. Li, Y. Wang, Z. Wang, Decolorization of azo dye by peroxymonosulfate activated by carbon nanotube: Radical versus non-radical mechanism, J Hazard Mater 320 (2016) 571-580.

[23] Y. Zhang, B. Wang, K. Fang, Y. Qin, H. Li, J. Du, Degradation of p-aminobenzoic acid by peroxymonosulfate and evolution of effluent organic matter: The effect of chloride ion, Chemical Engineering Journal 411 (2021) 128462.

[24] L. Gao, Y. Guo, J. Zhan, G. Yu, Y. Wang, Assessment of the validity of the quenching method for evaluating the role of reactive species in pollutant abatement

628 during the persulfate-based process, Water Res 221 (2022) 118730.
629 [25] X. Liu, Y. Hong, S. Ding, W. Jin, S. Dong, R. Xiao, W. Chu, Transformation of
630 antiviral ribavirin during ozone/PMS intensified disinfection amid COVID-19
631 pandemic, Sci Total Environ 790 (2021) 148030.
632 [26] Y. Yang, J.J. Pignatello, J. Ma, W.A. Mitch, Comparison of halide impacts on the
633 efficiency of contaminant degradation by sulfate and hydroxyl radical-based advanced
634 oxidation processes (AOPs), Environ Sci Technol 48 (2014) 2344-2351.
635 [27] S.-P. Tong, S. Yu, Y. Gao, C.-A. Ma, Effect of Inorganic Ions on the Oxidative
636 Efficiency of Ti(IV)-Catalyzed H_2O_2/O_3Process in the pH Range of 1.0 to 6.0, Ozone:
637 Science & Engineering 35 (2013) 359-365.
638 [28] L. Peng, Y. Shang, B. Gao, X. Xu, Co_3O_4 anchored in N, S heteroatom co-doped
639 porous carbons for degradation of organic contaminant: role of pyridinic N-Co
640 binding and high tolerance of chloride, Applied Catalysis B: Environmental 282 (2021)
641 119484.
642 [29] Z. Wang, R. Yuan, Y. Guo, L. Xu, J. Liu, Effects of chloride ions on bleaching of
643 azo dyes by Co^{2+}/oxone reagent: kinetic analysis, J Hazard Mater 190 (2011)
644 1083-1087.
645 [30] Y. Huang, F. Yang, L. Ai, M. Feng, C. Wang, Z. Wang, J. Liu, On the kinetics of
646 organic pollutant degradation with Co(2+)/peroxymonosulfate process: When
647 ammonium meets chloride, Chemosphere 179 (2017) 331-336.
648 [31] Y. Xue, Z. Wang, R. Naidu, R. Bush, F. Yang, J. Liu, M. Huang, Role of halide

649 ions on organic pollutants degradation by peroxygens-based advanced oxidation
650 processes: A critical review, Chemical Engineering Journal 433 (2022) 134546.
651 [32] Y. Lei, C.-S. Chen, J. Ai, H. Lin, Y.-H. Huang, H. Zhang, Selective decolorization
652 of cationic dyes by peroxymonosulfate: non-radical mechanism and effect of chloride,
653 RSC Advances 6 (2016) 866-871.
654 [33] Y. Lei, J. Lu, M. Zhu, J. Xie, S. Peng, C. Zhu, Radical chemistry of diethyl
655 phthalate oxidation via UV/peroxymonosulfate process: Roles of primary and
656 secondary radicals, Chemical Engineering Journal 379 (2020) 122339.
657 [34] Y.-H. Guan, J. Ma, D.-K. Liu, Z.-f. Ou, W. Zhang, X.-L. Gong, Q. Fu, J.C.
658 Crittenden, Insight into chloride effect on the UV/peroxymonosulfate process,
659 Chemical Engineering Journal 352 (2018) 477-489.
660 [35] L. Qin, H. Ye, C. Lai, S. Liu, X. Zhou, F. Qin, D. Ma, B. Long, Y. Sun, L. Tang,
661 M. Yan, W. Chen, W. Chen, L. Xiang, Citrate-regulated synthesis of hydrotalcite-like
662 compounds as peroxymonosulfate activator - Investigation of oxygen vacancies and
663 degradation pathways by combining DFT, Applied Catalysis B: Environmental 317
664 (2022) 121704.
665 [36] L. Qin, W. Chen, Y. Fu, J. Tang, H. Yi, L. Li, F. Xu, M. Zhang, W. Cao, D. Huang,
666 C. Lai, Hemin derived iron and nitrogen-doped carbon as a novel heterogeneous
667 electro-Fenton catalyst to efficiently degrade ciprofloxacin, Chemical Engineering
668 Journal 449 (2022) 137840.
669 [37] Z.Y. Li, L. Wang, Y.L. Liu, P.N. He, X. Zhang, J. Chen, H.T. Gu, H.C. Zhang, J.

Ma, Overlooked enhancement of chloride ion on the transformation of reactive species in peroxymonosulfate/Fe(II)/NH_2OH system, Water Res 195 (2021) 116973.

[38] S. Hou, L. Ling, D.D. Dionysiou, Y. Wang, J. Huang, K. Guo, X. Li, J. Fang, Chlorate Formation Mechanism in the Presence of Sulfate Radical, Chloride, Bromide and Natural Organic Matter, Environ Sci Technol 52 (2018) 6317-6325.

[39] J.K.S. Bruce C. Gilbert, and (in part) Wendy J. Peet and Karen J. Radford, Generation and Reactions of the Chlorine Atom in Aqueous Solution, J. Chem. SOC., Faraday Trans 84（10） (1988) 3319-3330.

[40] M.B.a.G.A.S. George V. Buxton, Reactivity of chlorine atoms in aqueous, J. Chem. Soc., Faraday T rans 94 (1998) 653-657.

[41] G.V. Buxton, C.L. Greenstock, W.P. Helman, A.B. Ross, Critical Review of rate constants for reactions of hydrated electrons, hydrogen atoms and hydroxyl radicals ($^{\cdot}OH/O^{\cdot-}$ in Aqueous Solution, Journal of Physical and Chemical Reference Data 17 (1988) 513-886.

[42] C.y.S. Ralf Mertens, Photolysis (A=254 nm) of tetrachloroethene in aqueous solutions Journal of Photochemistry and Photobiology A: Chemistry 85 (1995) 1-9.

[43] K. Hasegawa, P. Neta, Rate constants and mechanisms of reaction of chloride ($Cl_2^{\cdot-}$) radicals, The Journal of Physical Chemistry 82 (2002) 854-857.

[44] X. Cheng, H. Guo, Y. Zhang, X. Wu, Y. Liu, Non-photochemical production of singlet oxygen via activation of persulfate by carbon nanotubes, Water Res 113 (2017) 80-88.

691 [45] Y. Wang, D. Cao, X. Zhao, Heterogeneous degradation of refractory pollutants by
692 peroxymonosulfate activated by CoOx-doped ordered mesoporous carbon, Chemical
693 Engineering Journal 328 (2017) 1112-1121.
694 [46] E.T. Yun, J.H. Lee, J. Kim, H.D. Park, J. Lee, Identifying the Nonradical
695 Mechanism in the Peroxymonosulfate Activation Process: Singlet Oxygenation Versus
696 Mediated Electron Transfer, Environ Sci Technol 52 (2018) 7032-7042.
697 [47] Y. Yang, G. Banerjee, G.W. Brudvig, J.H. Kim, J.J. Pignatello, Oxidation of
698 Organic Compounds in Water by Unactivated Peroxymonosulfate, Environ Sci
699 Technol 52 (2018) 5911-5919.
700 [48] Y. Li, J. Li, Y. Pan, Z. Xiong, G. Yao, R. Xie, B. Lai, Peroxymonosulfate
701 activation on $FeCo_2S_4$ modified g-C_3N_4 ($FeCo_2S_4$-CN): Mechanism of singlet oxygen
702 evolution for nonradical efficient degradation of sulfamethoxazole, Chemical
703 Engineering Journal 384 (2020) 123361.
704 [49] S.Y. Wang, H. Jiao, Scavenging capacity of berry crops on superoxide radicals,
705 hydrogen peroxide, hydroxyl radicals, and singlet oxygen, J Agric Food Chem 48
706 (2000) 5677-5684.
707 [50] X.Y. Lou, Y.G. Guo, D.X. Xiao, Z.H. Wang, S.Y. Lu, J.S. Liu, Rapid dye
708 degradation with reactive oxidants generated by chloride-induced peroxymonosulfate
709 activation, Environ Sci Pollut Res Int 20 (2013) 6317-6323.
710 [51] Z. Wang, J. Li, W. Song, R. Ma, J. Yang, X. Zhang, F. Huang, W. Dong, Rapid
711 degradation of atrazine by a novel advanced oxidation process of bisulfite/chlorine

712 dioxide: Efficiency, mechanism, pathway, Chemical Engineering Journal 445 (2022)
713 136558.
714 [52] J. Callison, R. Edge, K.R. de Cuba, R.H. Carr, J.J.W. McDouall, D. Collison,
715 E.J.L. McInnes, W. van der Borden, K. van der Velde, J.M. Winfield, D. Lennon,
716 Origin of Impurities Formed in the Polyurethane Production Chain. 1. Conditions for
717 Chlorine Transfer from an Aryl Isocyanide Dichloride Byproduct, Industrial &
718 Engineering Chemistry Research 51 (2012) 2515-2523.
719 [53] A. Wang, B.Z. Zhu, C.H. Huang, W.X. Zhang, M. Wang, X. Li, L. Ling, J. Ma, J.
720 Fang, Generation mechanism of singlet oxygen from the interaction of
721 peroxymonosulfate and chloride in aqueous systems, Water Res 235 (2023) 119904.
722 [54] S. Garg, Y. Yuan, M. Mortazavi, T.D. Waite, Caveats in the Use of Tertiary Butyl
723 Alcohol as a Probe for Hydroxyl Radical Involvement in Conventional Ozonation and
724 Catalytic Ozonation Processes, ACS ES&T Engineering 2 (2022) 1665-1676.
725 [55] L. Hu, G. Zhang, M. Liu, Q. Wang, P. Wang, Enhanced degradation of Bisphenol
726 A (BPA) by peroxymonosulfate with Co_3O_4-Bi_2O_3 catalyst activation: Effects of pH,
727 inorganic anions, and water matrix, Chemical Engineering Journal 338 (2018)
728 300-310.
729 [56] X. Lu, X. Zhou, W. Qiu, Z. Wang, Y. Wang, H. Zhang, J. Yu, D. Wang, J. Gu, J.
730 Ma, Kinetics and mechanism of the reaction of hydrogen peroxide with hypochlorous
731 acid: Implication on electrochemical water treatment, J Hazard Mater 438 (2022)
732 129420.

733 [57] W. Yao, J. Fu, H. Yang, G. Yu, Y. Wang, The beneficial effect of cathodic
734 hydrogen peroxide generation on mitigating chlorinated by-product formation during
735 water treatment by an electro-peroxone process, Water Res 157 (2019) 209-217.
736 [58] D. Ghernaout, N. Elboughdiri, Disinfection By-Products (DBPs) Control
737 Strategies in Electrodisinfection, OALib 07 (2020) 1-14.
738 [59] D. Ghernaout, N. Elboughdiri, A. Alghamdi, B. Ghernaout, Trends in Decreasing
739 Disinfection By-Products Formation during Electrochemical Technologies, OALib 07
740 (2020) 1-17.
741 [60] S. Batterman, Quenching of chlorination disinfection by-product formation in
742 drinking water by hydrogen peroxide, Water Research 34 (2000) 1652-1658.
743 [61] X. Chen, W.-D. Oh, Z.-T. Hu, Y.-M. Sun, R.D. Webster, S.-Z. Li, T.-T. Lim,
744 Enhancing sulfacetamide degradation by peroxymonosulfate activation with N-doped
745 graphene produced through delicately-controlled nitrogen functionalization via
746 tweaking thermal annealing processes, Applied Catalysis B: Environmental 225 (2018)
747 243-257.
748 [62] C.G.a.P.P. J.-M. Herrmann, Heterogeneous photocatalysis : an emerging
749 technology for water treatment Catalysis Today 17 (1993) 7-20.
750 [63] C.X. Li, Y.J. Wang, C.B. Chen, X.Z. Fu, S. Cui, J.Y. Lu, H.Q. Liu, W.W. Li,
751 Interactions between chlorophenols and peroxymonosulfate: pH dependency and
752 reaction pathways, Sci Total Environ 664 (2019) 133-139.
753 [64] X. Li, S. Zhang, M. Yu, H. Xu, J. Lv, S. Yang, X. Zhu, L. Li, One-pot pyrolysis

754 method for synthesis of Fe/N co-doped biochar as an effective peroxymonosulfate
755 activator for RhB degradation, Journal of the Taiwan Institute of Chemical Engineers
756 128 (2021) 209-219.
757 [65] C. Fang, X. Lou, Y. Huang, M. Feng, Z. Wang, J. Liu, Monochlorophenols
758 degradation by UV/persulfate is immune to the presence of chloride: Illusion or
759 reality?, Chemical Engineering Journal 323 (2017) 124-133.
760